Carbon Nanotubes: Electronic Structure and Physical Properties☆

P Lambin, University of Namur, Namur, Belgium
VN Popov, University of Sofia, Sofia, Bulgaria

1	**Electronic structure**	1
1.1	π-Electron Zone-Folding Approximation	1
1.2	Electronic structure	2
1.3	Multiwall Nanotubes	3
2	**Transport Properties**	4
2.1	Landauer Conductance	4
2.2	Effect of Defects	4
2.3	Multiwall Nanotubes	5
3	**Other Properties**	5
3.1	Optical Properties	5
3.2	Transistor Effect	6
3.3	Field Emission	6
3.4	Mechanical Strength	7
4	**Summary**	8
References		8

Like for graphene, many physical properties of a nanotube depend on its remarkable electronic structure. Transport properties and optical properties of the nanotubes are, of course, directly linked to its electronic band structure. The response of a nanotube to an external field also depends on its electronic structure: field-effect transistor (FET) and field emission are two important phenomena taking place upon application of an electric field. All these aspects are discussed below.

1 Electronic structure

1.1 π-Electron Zone-Folding Approximation

Conceptually, a single-wall nanotube can be constructed by rolling up a graphene strip into a seamless cylinder. The basic construction is shown in **Figure 1(a)** where the universally used wrapping indices (n,m) are defined. The rolling-up operation brings the (n,m) node of the graphene sheet onto the origin O.

The starting point for understanding the electronic properties of a nanotube is the band structure of graphene. Close to the Fermi energy, the band structure of graphene is dominated by the p states formed by the interacting $2p_z$ orbitals normal to the atomic plane. Since graphene contains two atoms in its unit cell, there are two p bands, a bonding (π) one and an anti-bonding (π^*) one. In the linear combination of atomic orbital (LCAO) approximation (Wallace, 1947), the dispersion of these two bands in the two-dimensional reciprocal space of the wave vector $\mathbf{k}$ follows a simple analytical expression

$$E_{\pm}(k) = \varepsilon_\pi \pm \frac{\gamma_0 |F(k)|}{1 \mp S|F(k)|} \qquad [1]$$

where $\gamma_0 = |V - S\varepsilon_\pi|$, S and V being the overlap and hopping integrals between two nearest-neighbor $2p_z$ orbitals, respectively, and ε_π is the energy of these orbitals. The upper sign in eqn [1] is for the unoccupied π^* band, the lower sign is for the occupied π band, $F(\mathbf{k}) = 1 + \exp(i\mathbf{k}.\mathbf{a}_1) + \exp(i\mathbf{k}.\mathbf{a}_2)$ with $\mathbf{a}_1$ and $\mathbf{a}_2$ being the two primitive translation vectors of the graphene hexagonal lattice. The best values of the parameters in eqn [1] are $\gamma_0 = 2.9$ eV, $S = 0.13$.

The separation between the π^* and π bands in the reciprocal plane of graphene is represented in **Figure 1(b)**. These bands cross each other at the corners of the hexagonal first Brillouin zone, the K points, where the function $F(\mathbf{k})$ vanishes. For symmetry reasons, the Fermi level coincides with the energy ε_π of the band crossing. Graphene is a zero-gap semiconductor; its density of states at the Fermi energy E_F is zero and increases linearly on both sides of E_F.

☆*Change History*: March 2015. P. Lambin made the following changes: Correction of the author affiliation name, phone and fax numbers, e-mail address. Updated version of the text with corrections of a few terms. Inclusion of new recent references. Inclusion of a paragraph on the excitons in nanotubes. Inclusion of a new subsection on the mechanical properties of the nanotubes.

 doi:10.1016/B978-0-12-803581-8.02296-7

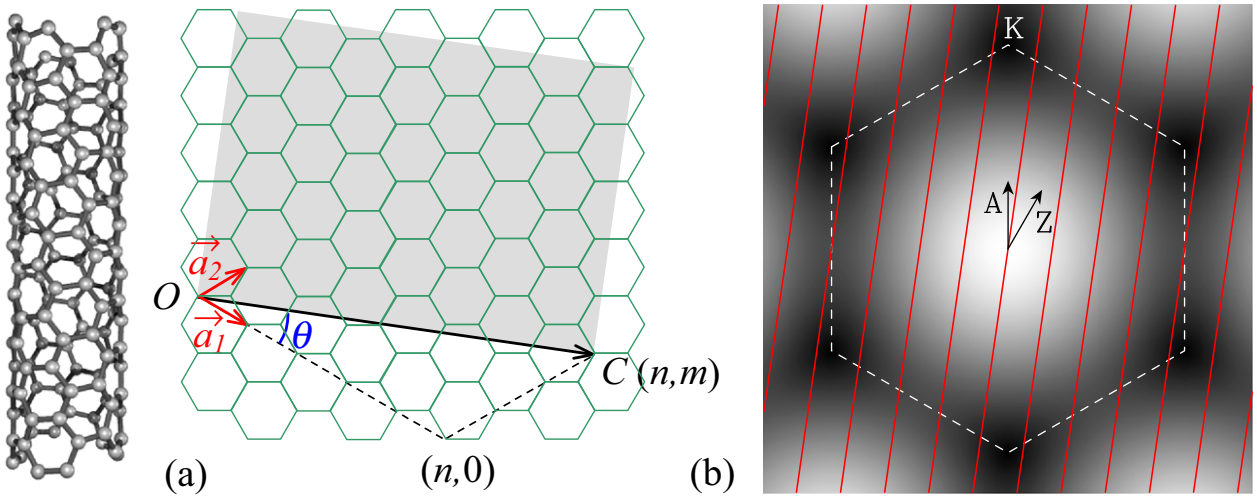

Figure 1 (a) Graphene sheet representing a planar development (shaded area) of the nanotube (*n*,*m*) for $n=5$ and $m=3$. θ is the chiral angle. In the rolled-up structure, *OC* is the circumference of the nanotube. (b) Gray-scale map of the separation between the π^* and π bands of graphene (black corresponds to 0, white to 6.9 eV) in the reciprocal plane of graphene. The Γ point is at the center of the figure. The boundaries of the first Brillouin zone are shown by the dashed lines. The thick lines across the drawing are discretization lines of the Bloch vector for the (5,3) nanotube, parallel to its axis. The two arrows indicate the axial direction of armchair (A) ($m=n$) and zigzag (Z) ($m=0$) nanotubes.

In a single-wall nanotube, cyclic boundary conditions apply around the circumference. In the planar presentation shown in **Figure 1(a)**, the circumference of the nanotube is a translation vector of graphene, $\mathbf{C}=n\mathbf{a}_1+m\mathbf{a}_2$ n and m being the wrapping indices. The nanotube obtaine is either achiral – armchair ($n=m$) and zigzag ($m=0$) – or chiral ($n\neq m\neq 0$). In the two-dimensional graphene sheet, the wave function at the end point of **C** is the one at the origin multiplied by the Bloch factor $\exp(i\mathbf{k}.\mathbf{C})$. Assuming that the graphene wavefunctions remain valid in the rolled-up structure (zone-folding approximation), these cyclic boundary conditions impose $\exp(i\mathbf{k}.\mathbf{C})=1$. This condition discretizes the Bloch vector **k** along equidistant lines $\mathbf{k}.\mathbf{C}=2\pi\ell$ perpendicular to **C** and therefore parallel to the nanotube axis, where ℓ is an integer number. These discretization lines are drawn in **Figure 1(b)**. Along each of these lines, the π and π^* bands of graphene are sampled. Both bands are always separated by a gap, unless a discretization line passes exactly through a corner *K* point of the first Brillouin zone. The nanotube is then a metal, because it contains two bands that cross the Fermi level. This happens when $nK_1+mK_2=\ell$, where K_1 and K_2 are the coordinates of a *K* point in the basis formed by the reciprocal unit vectors of graphene. Taking $K_1=1/3$ and $K_2=-1/3$ leads to the condition $n-m=3\ell$. In other words, $n-m$ must be a multiple of 3 to obtain a metallic nanotube, otherwise the nanotube is a semiconductor (Hamada *et al.*, 1992). An armchair nanotube (n=m) is always a metal. This can be seen directly from **Figure 1(b)**: a line drawn along the arrow marked A always intersects the upper *K* point of the first Brillouin zone.

The band gap of a semiconducting nanotube is easily calculated. Close to the *K* point, the function $F(\mathbf{k})$ can be linearized with respect to the distance $\delta\mathbf{k}$ of the wave vector **k** from the *K* point. To first order in $\delta\mathbf{k}$, eqn [1] simplifies in

$$E_{\pm}(\delta k)=\varepsilon_{\pi}\pm\frac{3}{2}\gamma_0 d_{CC}|\delta k| \qquad [2]$$

where d_{CC} is the carbon – carbon (CC) bond length of 0.14 nm. As can be seen in **Figure 1(b)**, the closest distance of the discretization lines to a *K* point for a semiconductor is one third the separation between these lines, which is the reciprocal of the nanotube radius. Setting $|\delta\mathbf{k}|=2/3d$, with d the nanotube diameter, in the above equation leads to the smallest possible energy of the π^* states and the largest possible value of the π states. The separation between them is the band gap, $E_g=2\gamma_0\ d_{CC}/d$. This formula is asymptotically correct for large d.

1.2 Electronic structure

For small diameter ($d<1.2$ nm), the linear and isotropic dependence of the energy of the π^* and π bands of (eqn [2]) is no longer valid even at the distance of closest approach of the discretization lines to the *K* point. Corrections to the $1/d$ dependence of the band gap are required, the obtained leading term being proportional to $-r\cos(3\theta)/d^2$. Here, θ is the chiral angle represented in **Figure 1(a)** and $r=+1$ or -1 is such that $n-m=M(3)+r$, where $M(3)$ means an integer multiple of 3. Furthermore, the π orbitals, being locally oriented along the normal to the nanotube, are not parallel to each other as in graphene. They mix with the σ orbitals of neighboring sites. This mixing, although small, lifts the degeneracy of the π and π^* states at the *K* point. A small gap

opens for these nanotubes for which $n-m=M(3)$, except for the armchair nanotubes where the crossing of the bands at ε_π is still allowed, due to the C_{nv} symmetry for all Bloch wave vectors.

More refined electronic theories are required to account for the curvature-induced effects, such as tight-binding models including all the valence electrons of C and *ab initio* techniques, generally based on the local density approximation. We show here below the results of a nonorthogonal tight-binding model that incorporates the 2s and 2p orbitals of carbon (Popov, 2004). The calculated band gap of all nanotubes with diameter smaller than 2.4 nm are represented by the lowest curve in **Figures 2(a)** and **(b)**. In **Figure 2(a)**, one clearly sees the rapid closing ($1/d^2$ law) of the gap upon increasing diameter of the 'pseudo-metallic'' nanotubes (those for which $n-m=M(3)\neq 0$). For $d>1.2$ mn, the band gap of the semiconducting nanotubes ($n-m=M(3)\pm 1$) shown by the lowest curve in **Figure 2(b)** follows reasonably well the $1/d$ law predicted by the zone-folding approximation. Below that diameter, the band gap becomes dependent on the chirality of the nanotube, as it can be observed in **Figure 2(b)**.

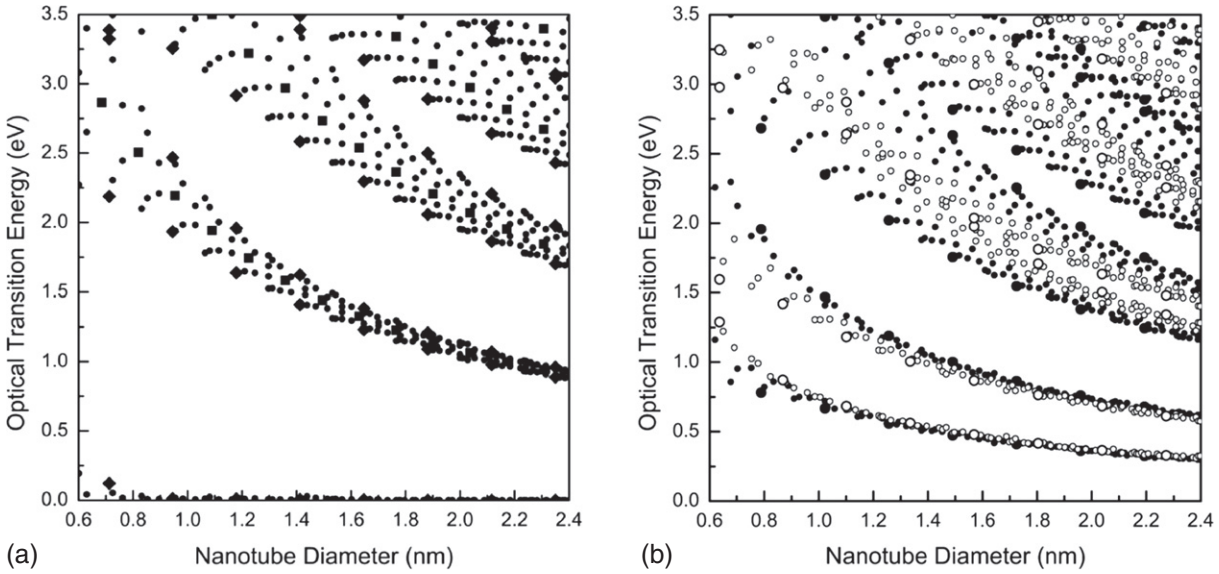

Figure 2 Optical transition energies computed with a nonorthogonal tight-binding model for (n,m) nanotubes with (a) $n-m=M(3)$ (metals) and (b) $n-m=M(3)+r$ (semiconductors) vs. diameter. In (a) squares are for armchair nanotubes ($m=n$), diamonds for zigzag tubes ($m=0$), and circles for chiral nanotubes ($0<m<n$). In (b), open symbols correspond to $r=$-1 and black symbols correspond to $r=+1$; large circles are for zigzag and small circles for chiral nanotubes.

The electron band structure represented against the one-dimensional wave vector and the density of states of two nanotubes, a metal and a semiconductor, are shown in **Figures 3(a)** and **(b)**. In the band structure of the metallic nanotube (**Figure 3(a)**), two branches derived from the π and π^* bands of graphene cross at the Fermi level. These branches have a nearly linear dispersion around the Fermi wave vector. According to eqn [2], their slope is $\hbar v_F = \pm 3\gamma_0 d_{CC}/2$ where v_F is the Fermi velocity. With the same approximation, the highest valence and lowest conduction bands of a semiconducting nanotube (**Figure 3(b)**) have a hyperbolic dispersion relation

$$E_\pm(k) = \varepsilon_\pi \pm \sqrt{(E_g/2)^2 + (3\gamma_0 d_{CC}/2)^2 (k-k_m)^2} \qquad [3]$$

where k_m is the wave vector in the one-dimensional first Brillouin zone of the nanotube where the band gap is located. A metallic nanotube has a nearly constant density of states around the Fermi level. This plateau is generated by the two linear bands that cross at the Fermi energy. The density of states of a nanotube is characterized by a series of asymmetric spikes, called Van Hove singularities, arising at energies of vanishing slope of the electronic bands. These singularities form a real fingerprint of the nanotube. Their positions can be measured by scanning tunneling microscopy (STS) (Wildoer *et al.*, 1998).

1.3 Multiwall Nanotubes

Roughly stated, the electronic properties of multiwall nanotubes resemble those of graphite, which is semimetallic, as indicated by valence-band photoemission spectroscopy. These nanotubes present a rich variety of transport properties, briefly discussed in a separate section below. In principle, a multiwall nanotube mixes metallic and semiconducting layers. The small inter-layer coupling and the diameter of the constituent layers being larger than a few nm (which means small band gaps) make that the distinction between metal and semiconductor is not as pronounced as for single-wall nanotubes. However, both semiconducting

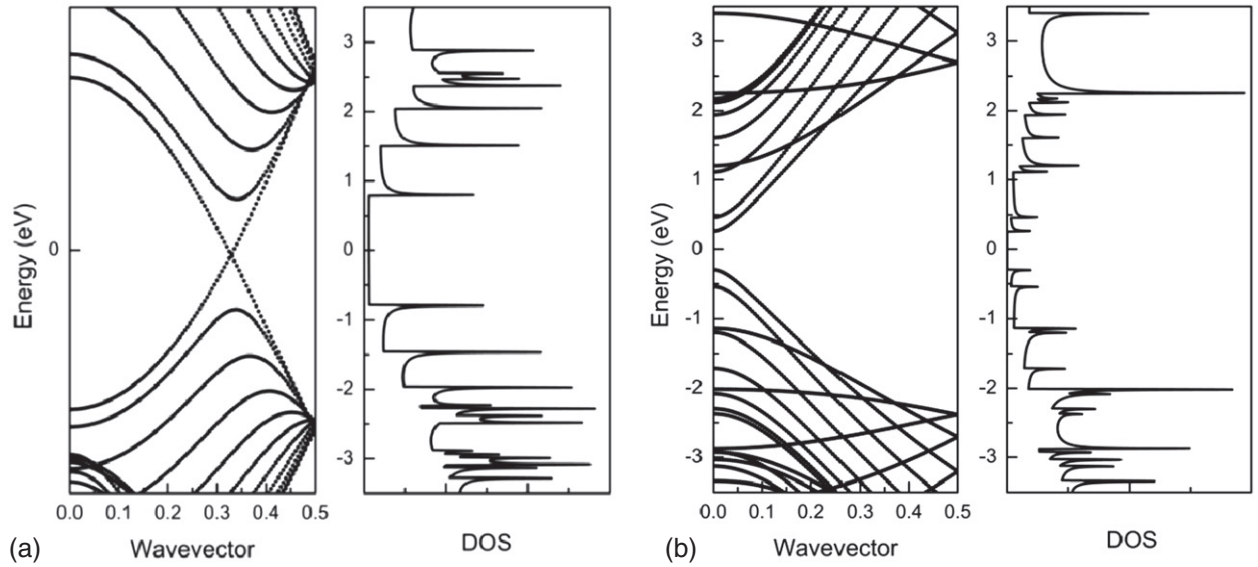

Figure 3 Electronic band structure and density of states of (a) the (10,10) armchair nanotube and (b) the (17,0) zigzag nanotube, computed with a nonorthogonal tight-binding model. The wave vector in the band structures is given in units of $2\pi/a$ with a the translational period of the nanotube.

and metallic characteristics were found by STS measurements performed on individual multiwall nanotubes. Furthermore, STS spectra may vary strongly from one place to another along the same tube, which may be due to the presence of defects. Defects such as pentagons, heptagons, impurities, and also bamboo-like structure with the compartmentation of the internal layers, affect the electronic properties of a nanotube. Different parts of it may have different electronic properties (Ebbesen *et al.*, 1996).

2 Transport Properties

2.1 Landauer Conductance

The transport properties of a single-wall nanotube (either a metal or a doped semiconductor) deviate significantly from Ohm's law because the charge carriers can flow ballistically over a large distance ($\sim 1\ \mu$m at room temperature), without suffering from inelastic scattering by phonons and defects. Even in the absence of any scattering of the charge carriers, the resistance of a nanotube is not zero. The reason for that is that the nanotube offers only a few propagating states in comparison with the macroscopic contact electrodes that have many such states. At small bias, the conductance of the nanotube is indeed controlled by the probability that an electron entering the nanotube from one electrode with Fermi energy E_F can be transmitted to any state with the same energy in the other electrode. The transmitted current is $I = GV$ with the differential conductance G given by

$$G = \frac{2e^2}{h}\sum_n T_n(E_F) \qquad [4]$$

Here the sum is over all nanotube electronic states n at the Fermi energy E_F that can carry a current in one direction, and T_n is the transmission probability for the conducting state n (also called a channel). Eqn [4] is the Landauer–Büttiker formula (Landauer, 1970). In the case of a perfect nanotube at zero temperature, $T_n = 1$ for all states, and $G = (2e^2/h)M$ with M the number of branches that cross E_F with a positive dE/dk slope. The electrical resistance is therefore $G^{-1} = h/(2e^2M) = 12.9/M$ kΩ. It is length-independent (ballistic transport) and quantized due to the finite number M of conducting channels. For a metallic nanotube $M = 2$ when E_F is close to the Fermi level ε_π. There are indeed two branches with positive slope crossing ε_π, one at a positive k (shown in **Figure 3(a)**), the other at the opposite wave vector $-k$. In practice, the resistance of a metallic nanotube can be significantly larger than 6.45 kΩ when there are poor electric contacts with the external electrodes. In addition, bending, squashing or twisting a nanotube may affect its conductivity, sometimes inducing a metal–semiconductor transformation.

2.2 Effect of Defects

The scattering of electrons by phonons and defects is expected to increase the electrical resistance. And indeed, the resistance of a nanotube increases slightly with increasing temperature above room temperature, due to the backscattering of electrons by

thermally excited phonons (Kane *et al.*, 1998). At low temperature, the resistance of an isolated metallic nanotube also increases *upon* cooling. This unconventional behavior for a metallic system may be the signature of electron correlation effects first observed in bundles of single-wall nanotubes (Luttinger liquid, typical of one-dimensional systems) (Bockrath *et al.*, 1999). A single impurity, like B or N, in a metallic nanotube affects only weakly the conductivity close to ε_π. The same holds true with a Stone–Wales defect, which transforms four adjacent hexagons in two pentagons and two heptagons. Interestingly, even long-range disorder induced by defects like substitutional impurities has a vanishing backscattering cross section in metallic nanotubes, at least when E_F is close to ε_π. This is not true with doped semiconducting nanotubes, where scattering by long-range disorder is effective.

2.3 Multiwall Nanotubes

The transport regime in multiwall nanotube is not as well established as for single-walled nanotubes. Experiment shows that they have a wide spectrum of transport properties. Some multiwall nanotubes are metallic or semimetallic, others are clearly non metallic. It is generally admitted that electron transport in a metallic multiwall nanotube at room temperature is not ballistic but instead, diffusive (Bachtold *et al.*, 2000). However, evidences also exist for ballistic transport taking place in the outermost shell of an individual nanotube in contact with a liquid metal (Frank *et al.*, 1998).

The room-temperature resistivity of annealed, large multiwall nanotubes is $2 \times 10^{-6}\ \Omega$ m and their resistance per unit length is typically 30 kΩ/μm. They can carry without failure a very large current density, up to 10^{11} A/m^2. By decreasing temperature below room value, the resistance of an individual nanotube generally increases slightly. At low temperature, this unconventional behavior is often interpreted as being the result of an increase of the elastic backscattering cross section of the electrons by defects, due to quantum interferences. This happens when the phase coherence length of the electrons, which increases upon cooling, becomes larger than the length of the nanotube.

3 Other Properties

3.1 Optical Properties

The optical properties of single-wall carbon nanotubes are mainly determined by electronic transitions between Van Hove singularities where there is a large accumulation of states in their density of states. For light polarized parallel to the nanotube axis, transitions between symmetric states with respect to the charge neutrality level ε_π are allowed. Among these, the transition across the direct band gap of the semiconducting nanotubes has the lowest energy. It correspond to a first optical absorption band at about $E_{11}^S = E_g \sim 0.6$ eV for usual nanotubes (those with diameter ~ 1.4 nm). The simple zone-folding approximation predicts another absorption band at about twice this energy E_{22}^S, still for the semiconducting nanotubes (see **Table 1**). As for the metallic single-wall nanotubes, the transition between the Van Hove singularities located on both sides of the metallic plateau of their density of states (see **Figure 3(a)**) has an energy E_{11}^M given in **Table 1**, which is typically 1.8 eV. Calculated optical transitions between 0.0 and 3.5 eV within the nonorthogonal tight-binding Hamiltonian are represented in **Figures 2(a** and **b)** for all single-wall nanotubes with diameter between 0.6 and 2.4 nm. The branch ending at 1 eV for $d = 2.4$ nm in **Figure 2(a)** represents the variations of E_{11}^M for metallic nanotubes. The lowest two curves in **Figure 2(b)** correspond to E_{11}^S and E_{22}^S in semiconductors. There is some spread of data point compared to the simple $1/d$ laws given in **Table 1**, which increases with decreasing diameter. The zigzag nanotubes deviate most from these simple laws.

Table 1 First optical transition energies in semiconducting and metallic nanotubes predicted by the π-electron zone-folding approximation (correct to first order in $1/d$, where d is the nanotube diameter)

Semiconductor			*Metal*
$E_{11}^S = 2\gamma_0 d_{CC}/d$	$E_{22}^S = 4\gamma_0 d_{CC}/d$	$E_{33}^S = 8\gamma_0 d_{CC}/d$	$E_{11}^M = 6\gamma_0 d_{CC}/d$

Spectrofluorimetry allows one to probe both first and second transition energies in semiconducting nanotubes. In this type of experiment, a nanotube is excited with a radiation of energy E_{22}^S and it reemits light of energy E_{11}^S, the excess of energy being relaxed in a non-radiative way provided the nanotubes are isolated from each other by surfactants in a solution, wrapping indices can be assigned to each measured pair of optical transition energies. The transition energies determined in this way are larger than the predictions of the nonorthogonal tight-binding model by 0.3 eV (Popov, 2004). For not too small diameters, the correction to the band-structure model is attributed to self-energy and excitonic effects.

In semiconducting nanotubes, excitonic effects modify the band-structure picture just described (Ajiki, 2012). An exciton is formed when an electron is transferred to the valence band by absorption of a photon energy. The Coulomb interaction between

the excited electron and the hole just created in the valence band reduces the excitation energy by a quantity that can be as much as 0.4 eV in a single-walled nanotube. On the other hand, the self-energy effects yield a substantial increase of the excitation energy. Both excitonic and self-energy effects result in an effective increase of the excitation energy by 0.3 eV relative to the band structure models. The above description of the optical properties of a nanotube remains qualitatively correct provided the transition energies E_{ii}^S refer to Van Hove singularities of the exciton band structure versus the wave vector of the electron-hole pair. In the excitonic picture, the ratio E_{22}^S/E_{11}^S can be significantly smaller than two (see **Table 1**), as observed experimentally.

Resonant Raman spectroscopy is another, widely-used characterization technique that can explore the optical properties of nanotubes. The Raman cross section is considerably enhanced when either the excitation light or the Raman scattered radiation matches an optical transition energy (Rao *et al.*, 1997). These are the conditions for having a resonant Raman scattering. For single-wall nanotubes, the radial breathing mode, that is, a Raman active vibration with uniform radial atomic displacements, is extremely useful for the characterization. This is because the angular frequency of this mode depends on the tube diameter, $\omega_{\mathrm{RBM}}=A/d$, with $A \sim 228\ \mathrm{cm}^{-1}$ nm (Liu *et al.*, 2012). By measuring ω_{RBM} versus laser energy for those nanotubes which are in resonance, two structural informations are obtained: the diameter (via ω_{RBM}) and the electronic transition energy (from the resonance condition), from which an (n,m) assignment can be performed (Fantini *et al.*, 2004). In resonant Raman spectroscopy of an individual nanotube, it is possible to identify the tube as being metallic or semiconducting from the shape of the tangential Raman band, located near $1580\ \mathrm{cm}^{-1}$, which is asymmetric in a metallic tube due to the coupling of this phonon band with plasmons.

3.2 Transistor Effect

The most spectacular potential application of semiconducting single-wall nanotubes in nanoelectronics is their use as a three-terminal device that works like a FET (Martel *et al.*, 1998; Tans *et al.*, 1998). In this application, a nanotube is attached to two metallic electrode lines, acting respectively as a source and a drain. The nanotube is separated from a third electrode, the gate, by a thin insulating layer, see **Figure 4(a)**. Due to the difference of work function between the nanotube and the electrodes, Shottky barriers are usually formed at the interfaces with the contacts. The valence and conduction bands of the nanotube are bent in order to adjust the Fermi level. Due to this band bending, the device has a very small conductivity for a small drain – source bias potential V_{DS} (see **Figure 4(b)**). The conductivity of the nanotube can be increased by several orders of magnitude by varying the gate voltage by a few volts above a threshold value. This is because the gate electric field reduces the bending of the bands of the nanotube. When it reaches the threshold value, the gate field aligns either the lowest conduction or the highest valence bands of the nanotube with the Fermi level of the drain or source electrodes, and a current starts flowing through the nanotube. Hence, depending on the gate potential, the transistor presents two states, OFF (low conductivity) and ON (high conductivity), as depicted in **Figure 4(b)**.

In today's FET devices, the insulating oxide layer between the gate and the nanotube is very thin. Thanks to the resulting high capacitive coupling to the nanotube, the gate signal can be amplified to a level such that the output voltage of a first transistor can control the input of a second one. This important technological improvement, plus the fact that both p-type, n-type, and ambipolar carbon nanotube FET transistors can be realized, makes it possible to integrate the nanotubes into elementary logical gates. At the time of writing, state-of-the art carbon nanotubes transistors present performances comparable to those of silicon metal-oxide semiconductor MOSFET transistors (Avouris, 2002). As demonstrated experimentally, carbon nanotubes make it possible to yield high-performance transistors, even with a channel length below 10 nm. At this length scale, they ouptperform the Silicon technology (Franklin *et al.*, 2012).

3.3 Field Emission

Due to their long aspect ratio (length to radius ratio), carbon nanotubes are suitable for electron field emission (de Heer *et al.*, 1995). The basic theory of field emission is the Fowler–Nordheim equation that strictly applies to a semi-infinite free-electron medium, with a triangular barrier at the surface given by $V(z)=E_{\mathrm{v}}-eFz$, where $z\ (>0)$ is the coordinate normal to the surface, E_{v} is the vacuum energy and F is the electric field. Using the Wentzel-Kramers-Brillouin (WKB) approximation for the tunneling probability across the barrier, the expression of the current is (in A)

$$I=\frac{1.5610^{-6}A}{\varphi}F^2\exp\left(-\frac{6.8310^{9}\varphi^{3/2}}{F}\right) \qquad [5]$$

where A is the emission area in m^2, F is in $\mathrm{V\,m}^{-1}$ and ϕ is the work function in eV. For single-wall nanotubes, ϕ is typically 4.8 eV, slightly more than for multiwall nanotubes for which ϕ is 4.6 eV. Setting for instance $A=5\times10^{-16}\ \mathrm{m}^2$ and $F=5\times10^{9}\ \mathrm{V\,m}^{-1}$ leads to $I=1.5$ nA

Thanks to the long aspect ratio of a nanotube, the local electric field F acting on the tip can be considerably larger than the applied field V/D where V is the applied voltage and D is the distance between the nanotubes and the collecting anode. In eqn [5], $F=\beta V/D$ must be used, where the so-called amplification factor β strongly depends on the type of nanotubes (single-wall, bundle

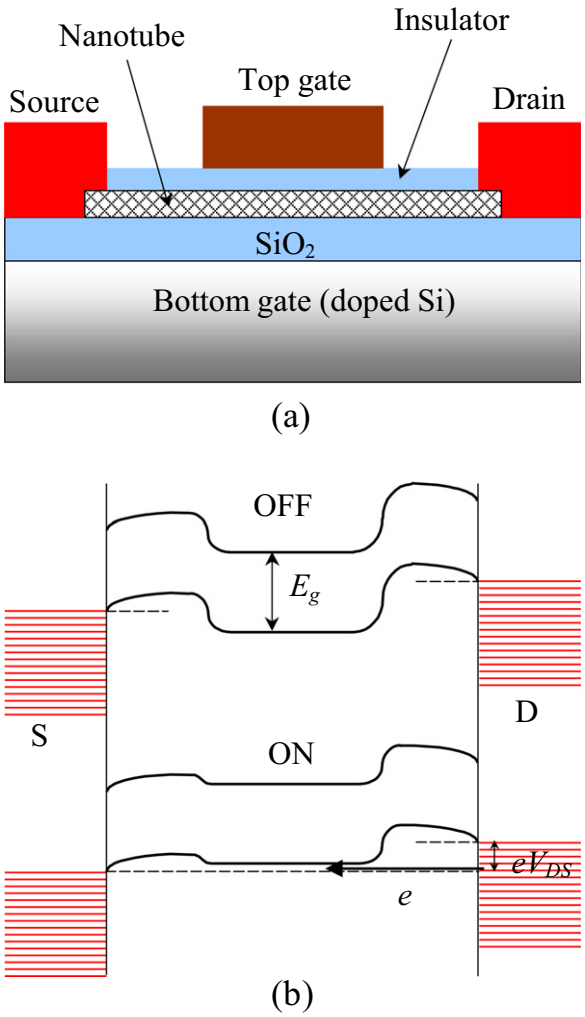

Figure 4 (a) Schematic representation of a nanotube field-effect transistor (FET) with its three metallic electrodes (source, drain and top gate). (b) Simplified band diagram showing the functioning of the FET supposed to be p-doped by field effect from the bottom gate. The source (S) and drain (D) electrodes are supposed to have a work function close to that of the semiconducting nanotube. A small positive potential V_{DS} is applied to the drain to bias the nanotube. The top gate has a smaller work function than the nanotube. When the top gate is at a zero or slightly negative potential V_{GS}, the transistor is in an OFF state due to the band bending. A negative V_{GS} potential moves the HOMO and LUMO bands of the nanotube upwards. In the ON state, electrons can flow from the drain to the source as indicated by the arrow marked with *e*.

of single-wall, or multiwall), on whether the tubes are open or not, and on the morphology of the nanotube array. For an isolated nanotube, $\beta \sim 3 + L/R$; experimentally, β is 200. In an array, there is a screening of the electric field when the density of nanotubes increases, which in principle reduces the amplification factor considerably compared to that of an isolated tube. Nevertheless, $\beta = 2000$ has been reported for some emitting nanotubes embedded in a film. Ideally, the distance between the nanotubes should be of the order of their length.

A great advantage of nanotubes for field-emission devices is that self-oriented arrays can be grown directly on a patterned electrode. The carbon nanotubes can work in normal vacuum conditions (10^{-6} torr) under a reasonable threshold field: 2–10 V μm^{-1} (applied field V/D). Closed multiwall nanotubes obtained by arc-discharge have the best performances (Bonard *et al.*, 1999). A film of multiwall nanotubes can sustain a current density of a 0.3 mA cm^{-2} for a long duration. A single nanotube can emit a stable current of a few microamperes.

3.4 Mechanical Strength

The sigma bonds confer remarkable mechanical properties to the carbon nanotubes, at least for tensile stress. Single-wall nanotubes are, in addition, extremely flexible. It is not a surprise, then, that these nanostructures are an interesting constituent for the making of composite materials. An important advantage is that polymer-based composites acquire a substantial electrical conductivity when they are loaded with carbon nanotubes at a concentration above the percolation threshold (a few vol%).

For single-wall nanotubes, macroscopic concepts like Young's modulus lose their meaning, although the latter is ofen used in the literature. A tensile or compressive axial strain ϵ increases the total energy of a single-wall nanotube by $\Delta E/S = C\epsilon^2/2$ where S is the surface of the rolled-up graphene strip and C, a well-defined quantity, is the stiffness constant. C is readily accessible to standard electronic band-structure calculations. Computed values of C are typically 350 N m^{-1}. If Young's modulus $Y = C/t$ is used instead, its value depends on the chosen nanotube wall thickness t. More important for applications, perhaps, is the breaking tensile strain that, for good-quality single-wall nanotubes, may exceed 13% (Chang *et al.*, 2010).

4 Summary

One of the most spectacular properties of single-wall carbon nanotubes is that they can be metallic or semiconducting depending on their exact atomic structure. Metallic nanotubes are remarkable ballistic conductors, even at room temperature, while semiconducting single-wall nanotubes may become performant FETs. The nanotubes are good electron emitters. They have remarkable mechanical properties. Expected commercial applications of nanotubes, including nanoelectronic and optoelectronic devices, light sources, panel displays, supercapacitors … (De Volder *et al.*, 2013) will exploit all the properties that are direct consequences of their atomic and electronic structures, and nanoscopic diameter.

References

Ajiki, H., 2012. Exciton states and optical properties of carbon nanotubes. J. Phys.: Condens. Matter 24, 1–25. 483001.
Avouris, Ph., 2002. Carbon nanotube electronics. Chem. Phys. 281, 429–445.
Bachtold, A., Fuhrer, M.S., Plyasunov, S., *et al.*, 2000. Scanned probe microscopy of electronic transport in carbon nanotubes. Phys. Rev. Lett. 84, 6082–6085.
Bockrath, M., Cobden, D.H., Lu, J., *et al.*, 1999. Luttinger-liquid behavior in carbon nanotubes. Nature 397, 598–601.
Bonard, J.M., Salvetat, J.P., Stockli, T., Forro, L., Chatelain, A., 1999. Field emission from carbon nanotubes: Perspectives for applications and clues to the emission mechanism. Appl. Phys. A 69, 245–254.
Chang, C., Hsu, I.K., Aykol, M., *et al.*, 2010. A new lower limit for the ultimate breaking strain of carbon nanotubes. ACS Nano 4, 5095–5100.
de Heer, W.A., Chatelain, A., Ugarte, D., 1995. A carbon nanotube field-emission electron source. Science 270, 1179–1180.
De Volder, M.F.L., Tawfick, S.H., Baughman, R.H., Hart, A.J., 2013. Carbon nanotubes: Present and future commercial applications. Science 339, 535–539.
Ebbesen, T.W., Lezec, H.J., Hiura, H., *et al.*, 1996. Electrical conductivity of individual carbon nanotubes. Nature 382, 54–56.
Fantini, C., Jorio, A., Souza, M., *et al.*, 2004. Optical transition energies for carbon nanotubes from resonant Raman spectroscopy: Environment and temperature effects. Phys. Rev. Lett. 93, 1–4. 147406.
Frank, S., Poncharal, Ph, Wang, Z.L., de Heer, W.A., 1998. Carbon nanotube quantum resistors. Science 280, 1744–1746.
Franklin, A.D., Luisier, M., Han, S.J., *et al.*, 2012. Sub-10 nm carbon nanotube transistor. Nano Lett. 12, 758–762.
Hamada, N., Sawada, S.I., Oshiyama, A., 1992. New one-dimensional conductors: Graphitic microtubules. Phys. Rev. Lett. 68, 1579–1581.
Kane, C.L., Mele, E.J., Lee, R.S., *et al.*, 1998. Temperature-dependent resistivity of single-wall carbon nanotubes. Europhys. Lett. 41, 683–688.
Landauer, R., 1970. Electrical resistance of disordered one-dimensional lattices. Phil. Mag. 21, 863–867.
Liu, K., Wang, W., Wu, M., *et al.*, 2012. Intrinsic radial breathing oscillation in suspended single-walled carbon nanotubes. Phys. Rev. B 83, 1–4. 113404.
Martel, R., Schmidt, T., Shea, H.R., Hertel, T., Avouris, Ph, 1998. Single- and multi-wall carbon nanotube field-effect transistors. Appl. Phys. Lett. 73, 2447–2449.
Popov, V.N., 2004. Curvature effects on the structural, electronic and optical properties of isolated single-walled carbon nanotubes within a symmetry-adapted non-orthogonal tight-binding model. New J. Phys. 6 (17), 1–17.
Rao, A.M., Richter, E., Bandow, S., *et al.*, 1997. Diameter-selective Raman scattering from vibrational modes in carbon nanotubes. Science 275, 187–191.
Tans, S.T., Verschueren, A.R.M., Dekker, C., 1998. Room-temperature transistor based on a single carbon nanotube. Nature 393, 49–52.
Wallace, P.R., 1947. The band theory of graphite. Phys. Rev. 71, 622–634.
Wildoer, J.W.G., Venema, L.C., Rinzler, A.G., Smalley, R.E., Dekker, C., 1998. Electronic structure of atomically resolved carbon nanotubes. Nature 391, 59–62.